

Functional imaging of ganglion and receptor cells in living human retina by osmotic contrast

Clara Pfäffle,^{1,2,*} Dierck Hillmann,^{1,2,3,*} Hendrik Spahr,^{1,2} Lisa Kutzner,^{1,2} Sazan Burhan,¹ Felix Hilge¹
and Yoko Miura,^{1,2,4} Gereon Hüttmann^{1,2,5}

¹ Institute of Biomedical Optics, University of Lübeck,
Peter-Monik-Weg 4, 23562 Lübeck, Germany

² Medical Laser Center Lübeck GmbH, Peter-Monik-Weg 4, 23562
Lübeck, Germany

³ Thorlabs GmbH, Maria-Goeppert-Straße 9, 23562 Lübeck, Germany

⁴ Department of Ophthalmology, University of Lübeck, Ratzeburger
Allee 160, 23562 Lübeck, Germany

⁵ Airway Research Center North (ARCN), Member of the German
Center of Lung Research (DZL), 35392 Gießen, Germany

*Both authors contributed equally

Imaging neuronal activity non-invasively in vivo is of tremendous interest, but current imaging techniques lack either functional contrast or necessary microscopic resolution. The retina is the only part of the central nervous system (CNS) that allows us direct optical access. Not only ophthalmic diseases, but also many degenerative disorders of the CNS go along with pathological changes in the retina. Consequently, functional analysis of retinal neurons could lead to an earlier and better diagnosis and understanding of those diseases. Recently, we showed that an activation of photoreceptor cells could be visualized in humans using a phase sensitive evaluation of optical coherence tomography data. The optical path length of the outer segments changes by a few hundred nanometers in response to optical stimulation. Here, we show simultaneous imaging of the activation of photoreceptor and ganglion cells. The signals from the ganglion cells are ten-fold smaller than those from the photoreceptor cells and were only visible using new algorithms for suppressing motion artifacts. This allowed us to generate a wiring diagram showing functional connections between photoreceptors and ganglion cells. We present a theoretical model that explains the observed intrinsic optical signals by osmotic volume changes, induced by ion influx or efflux. Since all neuronal activity is associated with ion fluxes, imaging osmotic induced size changes with nanometer precision should visualize activation in any neuron.

Introduction

Observing and investigating the activity and wiring of the central nervous system (CNS) in living humans can aid in a better understanding of neuronal function. Anatomically and developmentally the retina is part of the CNS. Therefore its neuron circuitry, its specialized immune response, and its blood-retina barrier resemble the respective parts of the CNS [1, 2]. Given these similarities, we may learn much about the CNS and peripheral nerves such as the spinal cord by imaging the retina [3]. Due to the optical properties of the eye the retina is directly accessible to optical imaging, with higher resolution (micrometer range) and more contrast options than magnetic resonance imaging (MRI), functional MRI (fMRI), or computed tomography (CT). This should allow a better diagnosis not only of neurodegenerative ophthalmic diseases like glaucoma or age-related macular degeneration (AMD), but also of diseases of the CNS. For example, the progress of neurodegenerative diseases like multiple sclerosis [4, 5, 6], Parkinson’s disease, [7, 8] or Alzheimer’s disease [9, 10, 11, 12, 13] correlates with morphological changes in specific retinal regions. Being the last neurons in the retinal circuitry, which transmit the visual information to the brain, the ganglion cells are of special importance. Interestingly, they show morphological changes in all above mentioned neurodegenerative disorders. In many of these, ocular manifestation even precedes symptoms in the brain, therefore eye investigation can offer earlier diagnosis [3]. It is reasonable to assume that, prior to morphological changes, neuronal function of the retina is corrupted or changed. But currently we are lacking methods to objectively check neuron function on a near cellular level in vivo.

The main reason is that activation potentials of the neurons yield only small optical changes [14, 15, 16, 17] and are therefore hard to detect. However, it has also been observed that the volume of excited neurons increases due to osmotic processes [18, 19, 20, 21], which elongate or shorten cell axes by tens of nanometers. Such

volume changes are orders of magnitude greater than optical path length changes induced by changes of the refractive index by varying ion concentrations. However, their detection is still challenging, because spatial changes are far below the resolution limit of current clinically used imaging methods like optical coherence tomography (OCT), ultrasound, or MRI. Moreover optical path length (OPL) changes of inevitable eye motion are orders of magnitude larger, corrupting measurements of osmotic changes.

Volumetric phase-sensitive imaging can observe length changes in the sub-wavelength range, provided that all motion related changes of the retina are compensated. We recently detected the activity of human photoreceptor cells (PRCs) after a light stimulus by using phase-sensitive parallel OCT imaging of the whole field of view with a fast tunable light source (Full-field swept-source OCT, FF-SS-OCT) [22]. The activation of the PRCs manifests itself in an elongation of the OPL of their outer segments (OS). Shortly after that, measurements by Zhang et al. showed a similar behavior in mice [23]. Based on these measurements, they introduced the idea that the observed OPL elongation may be caused by an osmotically driven volume increase, which mainly manifests in the axial dimension. Although an osmotically driven process fits well to the dynamics of our observations, this model leaves some questions unanswered: First, it is not obvious how the concentration of osmotically active molecules increases inside the photoreceptor OS to an extent that causes enough osmotic water influx. Second, it is unclear how the plasma membrane could resist the necessary dilation for the observed 10% increase in length. Finally, an inflow of water into the OS contradicts previous measurements showing that photoactivation increases the volume of the extracellular space (ECS) [19, 20].

So far, in human retinas functional responses have only been observed for the OS of photoreceptor cells, whereas no volume changes were seen in retinal neurons, such as the ganglion cells. However, concentration changes of ions causing osmotic effects are expected in these cells and their ECS as well, which should result in measurable volume changes.

Here, we show that ganglion cells indeed exhibit an expansion similar to the photoreceptor OS, albeit an order of magnitude smaller. By improving the correction of residual motion artifacts, we were able to simultaneously detect photoreceptor and ganglion cell activity. These data allowed us to map the wiring of photoreceptors to ganglion cells at different positions in the living human retina. Based on our data, we provide an alternative theoretical model to explain the observed change in photoreceptor OS and neuronal cells. This model considers the limited stretchability of biological lipid membranes,

relies on the molecular concentration change of ions during the hyperpolarisation, and is consistent with reported volume changes of the ECS.

Results and Discussion

The achievable axial resolution of OCT images is limited by the bandwidth of the light source and is typically a few micrometers. But in addition to the image intensity, the phases of the backscattered light are also acquired by interference and are sensitive to nanometer distance changes. However, in most OCT systems the phase information are corrupted by motion or scanning artifacts which render them worthless. Our FF-SS-OCT guaranteed phase stability and therefore allowed us to detect changes of the sample in the nanometer range. To image minute changes in the length of cone and rod OS, the phase differences between the inner segment outer segment junction (IS/OS) and the tips of the cone and rod OS were calculated, respectively. To detect changes of the OPL in the ganglion cells, we computed the phase difference between the ganglion cell layer (GCL), which contains the ganglion cell bodies, and the inner plexiform layer (IPL) with the synaptic connections from the ganglion cells with the bipolar and amacrine cells (Fig 1a). To measure smaller OPL changes on a background of more severe motion artifacts, as present in the GCL, we needed robust and sub-pixel precise post processing of the volumetric OCT data; the critical areas for the processing were segmentation, co-registration, correction of pulsation artifacts, and referencing the phase time course to a background signal.

With a sub-pixel precise segmentation and co-registration (see Methods), we were able to obtain phase stable measurements over more than 8 s. Afterwards, the first 5 volumes, in which no stimulation occurs and which correspond to 625 ms, were used for a dynamic phase referencing with a volume that was recorded in the same phase of the heart beat. This approach reduced motion artifacts due to the pulsation [24]. After dynamic phase referencing, the phase differences of the GCL and the IPL was still dominated by non periodic motion. However, averaging the phase differences over the whole stimulation time led to distinct recognizable stimulated areas. When extracting the phase time courses of those areas, the remaining motion artifacts were removed by averaging the phase difference of the background and subtracting it from the phase difference in the activated area. This post processing could finally extract time courses of the intrinsic optical signals (IOSs) between the GCL and the IPL .

As observed for the photoreceptor OS, the GCL shows an increase of the optical path length in the stimulated area. It is, however, an order of magnitude smaller. The

increase in OPL of the GCL reached its maximum of about 40 nm after approximately 5 s (Fig. 1a), whereas the elongation of the OS did not reach a saturation state after 8 s stimulation at a length dilatation of more than 290 nm for rods and 240 nm for cones (Fig. 1b). As expected, the activated area of the ganglion cells is laterally shifted with respect to the activated area of the photoreceptor OS as shown in Fig. 2. In addition to the lateral shift, a deformation of the activated area occurred. Both lateral shift and deformation are highest in direct neighborhood of the fovea. The mapped shift of the IOS shows a characteristic translation pattern (Fig. 2), the direction of this shift points radially outwards from the fovea, as was histologically shown before *ex vivo* by Drasdo et al. [25]. A larger shift near the fovea attributes to the absence of ganglion cells and the high density of cones in the fovea. In the case of our subject, the largest displacement is about 650 μm at 0.8 mm temporal, which agrees well with the results of Drasdo et al. (406 – 632 μm at 0.85 – 1.348 mm temporal); in 3 mm from the center of the fovea the shift is only about 180 μm . For the same stimulated area the activated area in the GCL is therefore larger near the fovea, because the receptive fields are smaller and each cone is connected to one individual ganglion cell, while in the periphery cone density decreases and the ganglion cells process information from several rods.

As it was suggested before [23] an osmotically driven volume change is a fitting explanation for the OPL elongation over hundreds of nanometers within several seconds. However, the largest concentration changes in photoreceptor cells and neurons are associated to changes of the membrane potential. During excitation, the neuron alters the permeability of its plasma membrane for specific ions, in order to shift the electrochemical equilibrium by a net influx of cations. This polarizes the membrane potential from negative to positive. But this rapid shift also changes the osmolarity in the cell and in the ECS, and therefore should lead to an osmotic water influx into the neuron. In contrast to neurons, stimulation of photoreceptor cells does not result in a depolarisation but in a hyperpolarisation of the plasma membrane [26]. The hyperpolarisation is caused by an inhibition of a dark current, which is caused by a permanent influx of cations into the cell. This dark current is compensated by an active transport of ions over the plasma membrane of the inner segment back into the ECS. The inhibition of the dark current therefore leads to a net efflux of cations into the ECS, which decreases the osmolarity of the photoreceptor cells and therefore should lead to a water efflux from the cells into the ECS. This different osmotic behavior of photoreceptor and ganglion cells after a light stimulus was already shown by Dmitriev et al. in chick retina [19]. They measured a volume increase of the

ECS around the photoreceptor cells, reaching its maximum after approximately 30 s; at the same time they observed the volume of the ECS decreasing around bipolar, amacrine, and ganglion cells, reaching saturation after about 5 s. In the ganglion cells, the measured IOS approach a saturation within 8 s of measurement time, too. Unfortunately, we could not generate reach phase stability over a longer measurement time and therefore did not observe a saturation of the photoreceptor elongation. Nevertheless, the general time courses of the photoreceptors and especially of the GCL that we obtained fit well to the ECS volume changes that Dmitriev et al. measured in the respective layers of chick retina.

At first glance, the postulated decrease of the OS volume contradicts an elongation of the photoreceptor OS. Indeed, the length of isolated OS shrinks by up to 40% under unphysiologically strong hypertonic conditions [27], but these measurements can arguably be transferred to physiological scenarios. The opposite, a significant elongation of the OS by an expanding volume would only be possible if accompanied by a significant increase of the membrane surface, but biological membranes are inelastic and rupture at about 3% dilation of their surface [28]. Furthermore, Cohen et. al observed that strong hypotonic conditions lead to a bulging of the OS, by which the diameter is increased and the length decreased [29]. Therefore, it is unlikely that cells compensate volume increase by a dilation of their plasma membrane. Instead, it is more likely that any physiological volume change is compensated by conformation, as, e.g., known from vesicles [30]. Following, we will show that the assumption of an osmotically driven volume decrease at constant and smooth surface area explains qualitatively and quantitatively the observed elongation of rod OS.

For simplicity we consider only the rod OS and assume a constant surface area. Since photoreceptor discs show no effect under different osmotic conditions [29], we expect cones to behave similarly, although we expect the kinetics of the process to be more complex. We describe the conically shaped rod OS as a biaxial ellipsoid, where the initial conformation has one long radius $a = 12.5 \mu\text{m}$ and two short radii $b = 1 \mu\text{m}$ [31]. The area surface of the ellipsoid is given by

$$A_{\text{ROS}} = 2\pi b \left(b + \frac{a^2}{\sqrt{a^2 - b^2}} \arcsin \left(\frac{\sqrt{a^2 - b^2}}{a} \right) \right)$$

and its volume is computed to

$$V_{\text{ROS}} = \frac{4}{3} \pi a b^2.$$

The surface area of the rod OS, A_{ROS} , computes to 124 μm^2 ; its initial volume to $V_{\text{ROS}} = 52.4 \mu\text{m}^3$. Assuming the surface area A_{ROS} to be constant, elongating the

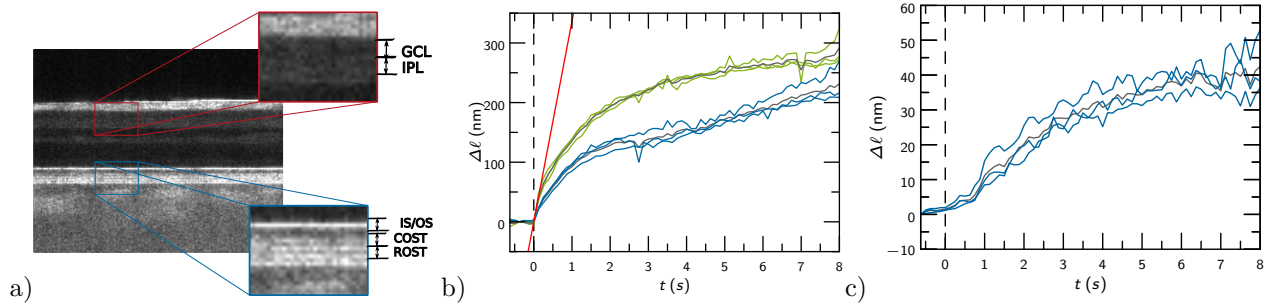


Figure 1: a) B-scan of the retina in 3 mm distance from the center of the macula. For the OPL of the cone and the rod OS, phase difference of the IS/OS junction (IS/OS, averaged over 2 px) and the cone OS tips (COST, averaged over 2 px) or the rod OS tips (ROST, averaged over 2 px) were calculated, respectively. For the OPL changes of the ganglion cells the phase differences between the GCL (GCL, averaged over 7 px) and the IPL (blue, averaged over 5 px) were determined. b) Optical path length (OPL) changes of cone (blue) and rod (green) OS. The averaged time course of those measurements are shown in grey. Initially, the rod OS elongates with a rate of 336 nm/s, as shown in red. c) OPL changes between GCL and IPL, which describes the optical distance of the ganglion cell bodies to their synapses for three different measurements (blue) and its averaged (black). All OPL changes were measured during 8 s stimulation in 3 mm distance from the center of the macula.

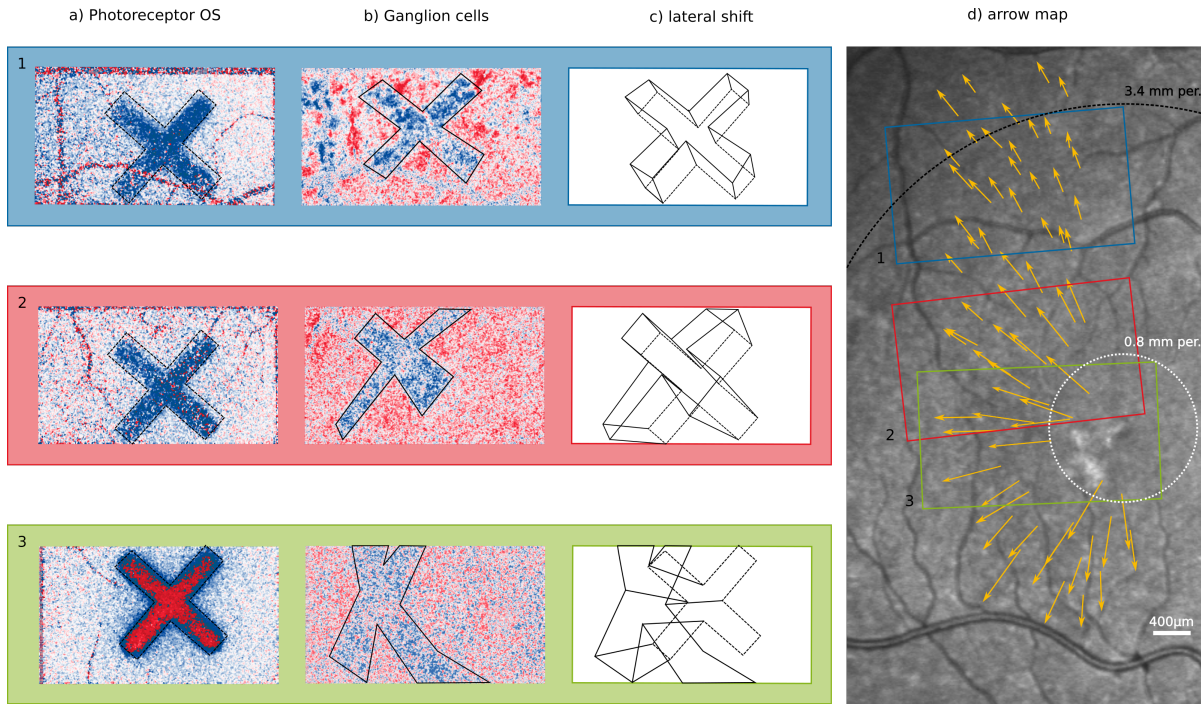


Figure 2: IOS pattern for different positions in the retina. Top row: in 3.5 mm superior temporal, center row: in 2 mm superior temporal and bottom row: in 1.8 mm temporal from the fovea. The positions correspond to the marked positions in the fundus image at the right. Column a) shows the observed pattern in the photoreceptor OS for each position and column b) in the GCL. Each pattern was outlined manually (Column c) and the corresponding edge points in the different layers were linked to generate the arrow map (Column d). An SLO image (Heidelberg engineering) of the subject is laid underneath the arrow map. The white and black circles mark the positions in 0.8 μm and 3.4 μm from the center of the macula, respectively.

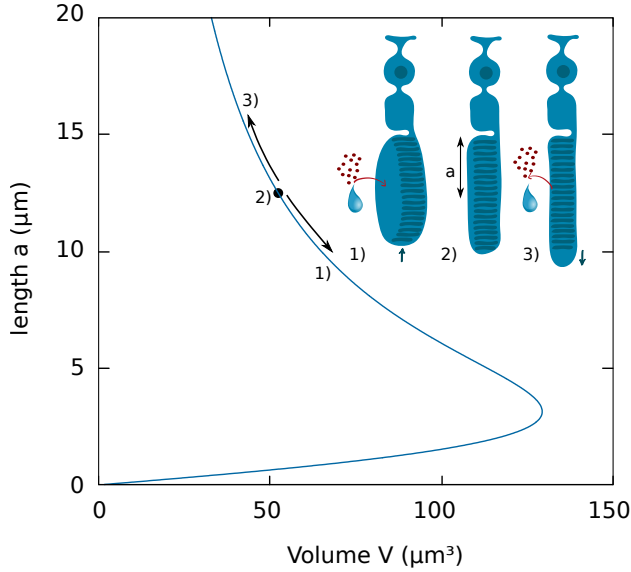


Figure 3: Volume V of biaxial ellipsoids with constant surface area ($124 \mu\text{m}^2$) as the length of its rotational axis a varies. Position (2) resembles the starting conditions of PRC OS with a vertical radius $a = 12.5 \mu\text{m}$ and volume of $52.4 \mu\text{m}^3$. Position (1): Decreasing the radius a leads to an increased volume. Position (3): Similarly, increasing the radius a decreases leads to a decreased volume.

long axis a will shrink the short axis b and thereby decrease the volume. In contrast, increasing the volume of the outer segment would shrink the long and elongate the short axis, thereby increasing the volume-to-surface ratio by getting closer to a spherical shape [29](Fig. 3).

To quantitatively characterize the process we consider the initial slope of the elongation of the OS, since at this point no saturation or other effects interfere with the dynamics of the process. The initial slope of the rod OS elongation ℓ is $\frac{d\ell}{dt} = 336 \frac{\text{nm}}{\text{s}}$; given a refractive index n of 1.41 [32], the long radius of the OS increases by $\frac{da}{dt} = \frac{1}{2n} \frac{d\ell}{dt} = 119 \frac{\text{nm}}{\text{s}}$. Assuming a constant surface area this results in a decreases of the short axis by $\frac{db}{dt} = 9.5 \frac{\text{nm}}{\text{s}}$ and a volume decrease with a rate of $\frac{dV_{\text{ROS}}}{dt} = 0.5 \frac{\mu\text{m}^3}{\text{s}}$.

To check if this volume change is consistent with the concentration change during the excitation of the PRCs, we need to determine the ion flux due to the stimulation. In our experiments, the stimulus intensity P is $27.5 \mu\text{W}$ at a central wavelength λ_0 of 550 nm and illuminates an area A_{stimulus} of about 1.3 mm^2 on the retina. For a mean photon energy $E = \frac{hc}{\lambda_0}$, with h being the Planck constant and c being the speed of light, this corresponds to a photocurrent density of $P/EA = 5.86 \times 10^7 \text{ s}^{-1} \mu\text{m}^{-2}$. After correcting for corneal reflection (4%), ocular media absorption (50%), and photons passed through the retina without being absorbed (80%) [33], $5.6 \times 10^6 \text{ s}^{-1} \mu\text{m}^{-2}$ photons remain for activation of the photoreceptor OS. This

photon flux saturates the rods and therefore yields the maximum ion current, which is $I_{\text{max}} = 13 \text{ pA}$ in human rods [31]. It is caused by the stimulus-induced inhibition of the dark-current, which is mainly composed of single charged Na^+ ($r_{\text{Na}^+} = 80\%$), but also double charged Ca^{2+} ($r_{\text{Ca}^{2+}} = 15\%$) and Mg^{2+} ($r_{\text{Mg}^{2+}} = 5\%$) [26]. The resulting concentration change rate $\frac{dc_{\text{ion}}}{dt}$ in the photoreceptor OS is thus computed to

$$\frac{dc_{\text{ion}}}{dt} = \frac{I_{\text{max}}}{e \cdot N_A \cdot 0.5 \cdot V_{\text{ROS}} \cdot (r_{\text{Na}^+} + 2r_{\text{Ca}^{2+}} + 2r_{\text{Mg}^{2+}})},$$

with e being the elementary charge, N_A the Avogadro constant, and V_{ROS} the volume of the rod OS. Due to the dense packaging with discs only half of the volume is filled with solvent, accounting for the factor 0.5 in the formula. The ion concentration increases by 4.28 mOsM/s , corresponding to $1.42 \frac{\%}{\text{s}}$ of the physiological osmolarity of 300 mOsM [34]. According to Van't Hoff law and assuming this concentration change is completely compensated by a volume change, this results in a rate of volume change rate of the same relative size ($\frac{dV}{dt} = 1.42 \frac{\%}{\text{s}} \times 0.5 \cdot V_{\text{ROS}} = 0.374 \frac{\mu\text{m}^3}{\text{s}}$), which is close to the value we calculated based on the observed length change in the OS ($0.5 \frac{\mu\text{m}^3}{\text{s}}$).

For the ganglion cells we expect an opposite volume change, since a decrease of the ECS volume was observed by Dmitriev et al. The phase evaluation, however, shows an elongation of the OPL in both layers. Here the situation is less clear than for the OS for two reasons: First, since the ganglion cells have a nearly spherical cell body, it is difficult to predict in which direction the cells will elongate in case of a volume increase. And second, the path length changes were measured not only over the cell bodies but included the synaptic endings of the ganglion cells. Therefore the phase changes do not necessarily correspond to an elongation of the cell bodies, but may also be explained by an expanding distance of these two structures.

Still, the general time course, magnitude, and saturation of the IOS in the GCL fit well to the observed volume change of Dmitriev et al. [19]. For this reason, we are confident that the OPL changes are also osmotically driven conformation changes of the ganglion cells.

Conclusion

Here, we demonstrate the non-invasive, simultaneous measurements of photoreceptor and ganglion cell activity after optical stimulation with high spatial and temporal resolution in the living human eye. Currently, we lack sensitivity as well as lateral and axial resolution to resolve single ganglion cell activity. However, as technology for phase stable imaging on a cellular level improves

[35] we expect investigations of single ganglion cell behavior in the living human eye to become possible in the near future. This will allow studying of neuron networks and information processing in the retina and even the brain. Future investigations will also have to show the value of this functional imaging for clinical diagnostics. Given the increasing clinical use of subtle morphological changes in the retina for diagnosing neuronal disorders, it is well possible that functional single neuron imaging will turn to an important tool there.

Our theoretical model gives an explanation for the molecular origin of our signals, which is consistent with earlier investigation of the PRC regarding concentration and volume changes. Nevertheless, we are aware that this explanation is currently based on a simple theoretical model and needs further experimental validation. The analysis of our results suggests that neuronal activity is visible by osmotic fluid changes between the ECS and the neuronal cell as it was observed earlier in chick eyes by Dmitriev et al [19]. Consequently, using osmotic contrast we should be able to observe activity in the bipolar and amacrine cell layers as well. One of our next tasks will be the visualization of OPL changes in this region to complete the functional imaging of the neuronal retina.

Acknowledgments

This research was funded by the German Research Foundation (DFG), project Holo-OCT HU 629/6-1.

Competing interests

D.H. works at Thorlabs GmbH, which manufactures and sells OCT devices.

Material and Methods

Setup and data acquisition The retina was imaged with a full-field swept-source OCT (FF-SS-OCT) system based on a Mach-Zehnder type interferometer (Fig. 4). The light of a swept source (Superlum BroadSweeper BS 840-1, central wavelength 841.5 nm, 51 nm sweep range) was split into reference and sample beam. The reference beam was collimated and brought onto the sensor of a high-speed camera (FASTCAM SA-Z, Photron). The sample beam illuminated the retina with a parallel beam at an irradiation power of 5.2 mW. The backscattered light was imaged onto the camera, where it was superimposed with the reference beam. The central 640×368 pixels of the camera were read out at a frame rate of 60 kHz. During one wavelength sweep, 512 images were recorded to acquire one volume in 8.5 ms. This corresponds to an A-scan rate of 27.6 MHz. With these parameters, 70 volumes could be acquired until the memory

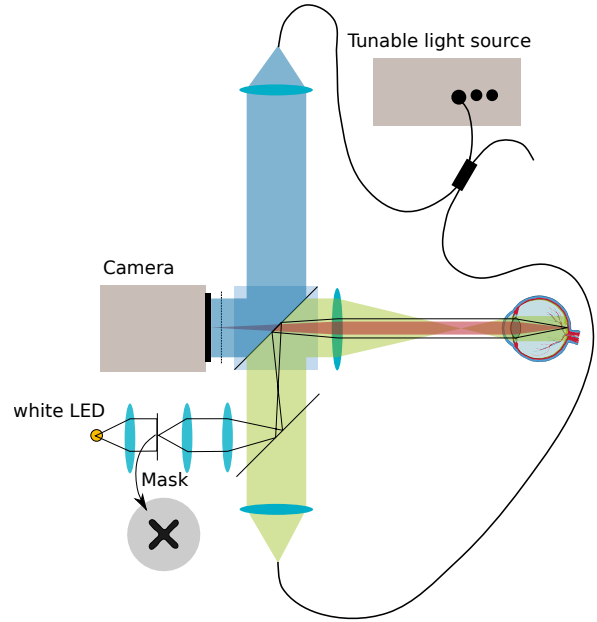


Figure 4: Setup for imaging photoreceptor and ganglion cell activity. The retina of the subject is illuminated with a collimated beam (green) and then imaged onto the sensor of a high-speed 2D camera, where it is superimposed with a collimated reference beam (blue). The stimulation of the retina is done by a white LED with an 'x'-shaped mask in the image plane, coupled into the sample illumination via a cold light mirror.

of the camera was exhausted, corresponding to a total measuring time of 0.595 s at full duty cycle. For longer measurements, the acquisition of a volume was only triggered every 125 ms, which enabled a total measurement time of 8.75 s. Although longer measurements are theoretically possible with this setup, we could not maintain phase stability for longer times, because speckle patterns and phases decorrelated too strongly.

The volumes were first reconstructed from the camera data as described in previous publications [22]. While lateral phase stability in one volume was achieved by the parallel imaging of all lateral positions, the axial phase error was effectively corrected via an optimization of image quality [36]. To achieve phase stability of the OCT data between volumes, their positions were aligned with sub-pixel precision to cancel phase changes due to bulk motion. This was achieved by a suitable co-registration and segmentation of the acquired volumes. For the stimulation of the retina white light was used, which was coupled into the sample beam via a cold mirror. A mask illuminated by the white LED was imaged onto the retina leading to an 'x'-shaped stimulation pattern, Total irradiation power was 27.5 μ W. For more detailed description of the setup see [22]

All investigations were done with fully dark adapted

healthy volunteers with a medically dilated pupil of 8 mm; written informed consent was obtained from all subjects. Compliance with the maximum permissible exposure (MPE) of the retina and all relevant safety rules was confirmed by the safety officer. The study was approved by the ethics board of the University of Lübeck (ethics approval Ethik-Kommission Lübeck 16-080)

Co-registration To co-register the volumes, three major steps were performed: A lateral coarse registration, a lateral fine registration, and an axial registration. For each step, we computed the deformation with respect to a master volume and individually corrected each volume.

For the lateral coarse registration, we laterally divided the volumes into tiles of size 256×256 pixels. The magnitude of the complex-valued OCT signal of each tile were then Fourier transformed in z -direction and again their magnitude was computed. This step removed any dependence of the z -position, which would otherwise be encountered as a z -dependent phase due to the Fourier shift theorem. Additionally, we cut off the lower 10% of all axial frequencies to remove high-frequency noise. These data were then phase correlated to determine the lateral x and y displacement between the respective tiles of two volumes that are compared. Finally, the median of all resulting x and y displacements between the respective and the master volume were taken to determine the coarse displacement.

The lateral fine registration was performed to also take deformations of the volumes into account. For this, tiles of size 128×128 pixels were created. Their correlation was computed in analogy to the previous step, but instead of taking the median, the displacements were interpolated to the full volume to give a displacement map as a function of the lateral position. To correct the displacements, an algorithm for a fast Fourier transform on non-equispaced data [37] in x and y direction was used to compute the correctly interpolated Fourier representation for all depth layers of the volume. A standard FFT to get back to position space gave interpolated results.

Finally, to obtain an axial displacement map, we divided into tiles of 96×96 pixels. The point-by-point magnitudes of the complex-valued tiles were phase correlated and the maximum of the phase correlation gave a z -displacement between the respective tiles of the two volumes. An interpolation upscaled the z -displacement map to give suitable values for all lateral points. Finally, we used these values to shift each A-scan in each volume axially by applying the Fourier shift theorem.

Segmentation Segmentation of FF-SS-OCT data with sub-pixel precision, faced two major challenges. First of all, the FF-SS-OCT images suffer from poor signal-to-noise ratio (SNR), and second, the data size is huge

(70 volumes, $640 \times 368 \times 256$ pixels each), leading to long computation times. Therefore an algorithm was needed that is robust against noise and evaluates in reasonable time. We achieved this by a combination of coarse graining, diffusion maps [38], and k -means clustering; the basic idea for this was previously proposed by Raheleh Kafieh et al. [39]. After co-registering all 70 volumes, they were averaged and only the mean volume was segmented; this reduced the data size and improved the SNR. In our case, the structure of interest was the inner segment/outer segment junction, which is a relatively smooth surface. Therefore, it is possible to coarse grain the volume of size $640 \times 368 \times 256$ to further reduce data size. In our case $10 \times 10 \times 1$ voxels were concentrated in one single voxel; the value of this resulting voxel was computed as the average intensity of this area. Afterwards, for each A-scan the four highest local maxima were extracted, which are characterized by their x , y , and z coordinate. Given these data points, we created a transition probability matrix between any two points that are separated by Δx , Δy , and Δz (measured in units of pixels). It is given by

$$\mathbf{p} = \begin{cases} G_{\sigma_r, \sigma_\theta}(r, \theta), & \Delta x \leq 1 \text{ and } \Delta y \leq 1 \text{ and } \Delta z \leq 1 \\ 0 & \text{otherwise} \end{cases}$$

where $r = \sqrt{\Delta x^2 + \Delta y^2 + \Delta z^2}$, $\theta = \cos^{-1}(\Delta z/r)$, and $G_{\sigma_r, \sigma_\theta}$ is a Gaussian function in two dimensions with covariance matrix $\text{diag}(\sigma_r^2, \sigma_\theta^2)$. With this matrix, transitions are only allowed for neighboring data points and lateral transitions are more likely than axial transitions. In a next step, a diffusion map of these data points was calculated [38]. The diffusion map maps the original data points to a new coordinate system depending on the transition probability matrix; in the new coordinate system points are closer together, if they have a high transition probability after a specified number of transitions N . We used $N = 10,000$ to reach a stationary state. Finally, a k -means clustering of the data points based on their distance in the diffusion coordinate system is done giving clusters, one of which corresponds to the IS/OS layer. The cluster of the IS/OS were used for a surface fit. Afterwards, each A-scan in all volumes is axially shifted by the Fourier shift theorem to align the IS/OS-surface to a constant depth.

Phase evaluation The phases in recorded volumes do not carry information about absolute position and can only measure changes when compared to phases in other layers and at other times. To cancel this arbitrary phase offset in each pixel the reconstructed volumes were first referenced to a volume before the start of the optical stimulus. For the evaluation of the phase differences the

complex OCT signal was averaged over several layers. Changes in the OPL of the photoreceptor outer segments were calculated from the phase difference of the inner segment/outer segment junction (averaged over 2 layers) and the outer segments tips (averaged over 2 layers) located 4 pixel deeper for cones and 6 pixel deeper for rods. For the evaluation of the ganglion cells the phase difference of the GCL (averaged over 6 pixels) and the IPL (averaged over 5 pixel) was calculated. The layer thickness of the GCL and IPL varies with the lateral position in the retina. Therefore the distance between those two layers is not fixed and needed to be chosen manually for each position individually (Fig. 1). Since retinal vessels are in the depth of the GCL, the phase difference are dominated by motion artifacts due to pulsation of the vessels. To minimize those artifacts each volume was referenced to one of the five volumes acquired before stimulation, which provides the smallest phase noise. This is the case if the reference volume is in a similar phase of the retinal heart-beat induced pulsation. The phase error for each possible reference volume was therefore determined by the standard deviation of the phase difference histogram. The image quality was improved by applying a lateral Gaussian filter to the complex data. Averaging over the whole stimulation time (5th - 70th volume) further improved the image quality of the response of the GCL (Fig. 2b). The images of the response of the photoreceptor OS were calculated only from the 20th volume (after 1875 ms of stimulation). The time-courses of the response of rods and cones were calculated from areas, which were selected manually (Fig. 2a). Averaging over this area improved signal quality. For phase changes larger than π the phase was unwrapped. OPL changes were calculated by

$$\Delta\ell = \frac{\Delta\Phi}{4\pi}\lambda_0.$$

In the GCL the time-course of the IOS was corrupted by inhomogeneously varying background changes in the phase, which were not connected to the optical stimulation. This background changes were removed by manually masking the area where the IOS arose and the vessels dominated the phase. The phase in the remaining background area was averaged, unwrapped and subtracted from the time course received from the IOS, before it was rescaled to length information.

To create the lateral translation map between photoreceptors and ganglion cells (Fig. 2c), the stimulation response in each image was outlined manually. Corresponding corners of the cross in each outline were then connected giving the results shown in Fig. 2c.

Data Availability The data that support the findings of this study are available from the corresponding author

upon reasonable request.

References

- [1] Kaur, C., Foulds, W. & Ling, E. Blood–retinal barrier in hypoxic ischaemic conditions: Basic concepts, clinical features and management. *Progress in Retinal and Eye Research* **27**, 622 – 647 (2008).
- [2] Streilein, J. W. Ocular immune privilege; therapeutic opportunities from an experiment of nature. *Nature Reviews Immunology* **3**, 879 – 889 (2003).
- [3] London, A., Benhar, I. & Scharz, M. The retina as a window to the brain—from eye research to CNS disorders. *Nature Reviews Neurology* **9**, 44 – 53 (2012).
- [4] Fisher, J. B. *et al.* Relation of visual function to retinal nerve fiber layer thickness in multiple sclerosis. *Ophthalmology* **113**, 324 – 332 (2006).
- [5] Green, A. J., McQuaid, S., Hauser, S. L., Allen, I. V. & Lyness, R. Ocular pathology in multiple sclerosis: retinal atrophy and inflammation irrespective of disease duration. *Brain* **133**, 1591 – 1601 (2010).
- [6] Monteiro, M. L. R., Fernandes, D. B., Apóstolos-Pereira, S. L. & Callegaro, D. Quantification of retinal neural loss in patients with neuromyelitis optica and multiple sclerosis with or without optic neuritis using Fourier-domain optical coherence tomography. *Investigative Ophthalmology & Visual Science* **53**, 3959 (2012).
- [7] Devos, D. *et al.* ERG and anatomical abnormalities suggesting retinopathy in dementia with Lewy bodies. *Neurology* **65**, 1107 – 1110 (2005).
- [8] Archibald, N. K., Clarke, M. P., Mosimann, U. P. & Burn, D. J. The retina in Parkinson’s disease. *Brain* **132**, 1128 – 1145 (2009).
- [9] Danesh-Meyer, H. V., Birch, H., Ku, J. Y.-F., Carroll, S. & Gamble, G. Reduction of optic nerve fibers in patients with Alzheimer disease identified by laser imaging. *Neurology* **67**, 1852 – 1854 (2006).
- [10] Blanks, J. C., Hinton, D. R., Sadun, A. A. & Miller, C. A. Retinal ganglion cell degeneration in Alzheimer’s disease. *Brain Research* **501**, 364 – 372 (1989).
- [11] Blanks, J. C., Torigoe, Y., Hinton, D. R. & Blanks, R. H. Retinal pathology in Alzheimer’s disease. I. ganglion cell loss in foveal/parafoveal retina. *Neurobiology of Aging* **17**, 377 – 384 (1996).

- [12] Blanks, J. C. *et al.* Retinal pathology in Alzheimer's disease. II. regional neuron loss and glial changes in GCL. *Neurobiology of Aging* **17**, 385 – 395 (1996).
- [13] Parisi, V. *et al.* Morphological and functional retinal impairment in Alzheimer's disease patients. *Clinical Neurophysiology* **112**, 1860 – 1867 (2001).
- [14] Berlind, T., Pribil, G. K., Thompson, D., Woollam, J. A. & Arwin, H. Effects of ion concentration on refractive indices of fluids measured by the minimum deviation technique. *Physica Status Solidi c* **5**, 1249 – 1252.
- [15] Hill, B., Schubert, E., Nokes, M. & Michelson, R. Laser interferometer measurement of changes in crayfish axon diameter concurrent with action potential. *Science* **196**, 426 – 428 (1977).
- [16] Iwasa, K., Tasaki, I. & Gibbons, R. Swelling of nerve fibers associated with action potentials. *Science* **210**, 338 – 339 (1980).
- [17] Oh, S. *et al.* Label-free imaging of membrane potential using membrane electromotility. *Biophysical Journal* **103**, 11 – 18 (2012).
- [18] Holthoff, K. & Witte, O. Intrinsic optical signals in vitro: a tool to measure alterations in extracellular space with two-dimensional resolution. *Brain Research Bulletin* **47**, 649 – 655 (1998).
- [19] Dmitriev, A., Govardovskii, V., Schwahn, H. & Steinberg, R. Light-induced changes of extracellular ions and volume in the isolated chick retina-pigment epithelium preparation. *Visual Neuroscience* **16**, 1157 – 1167 (1999).
- [20] Huang, B. & Karwoski, C. Light-evoked expansion of subretinal space volume in the retina of the frog. *Journal of Neuroscience* **12**, 4243–4252 (1992).
- [21] Holthoff, K. & Witte, O. Intrinsic optical signals in rat neocortical slices measured with near-infrared dark-field microscopy reveal changes in extracellular space. *Journal of Neuroscience* **16**, 2740 – 2749 (1996).
- [22] Hillmann, D. *et al.* In vivo optical imaging of physiological responses to photostimulation in human photoreceptors. *Proceedings of the National Academy of Sciences* **117**, 13138 – 13143 (2016).
- [23] Zhang, P. *et al.* In vivo optophysiology reveals that g-protein activation triggers osmotic swelling and increased light scattering of rod photoreceptors. *Proceedings of the National Academy of Sciences* **114**, 2937 – 2946 (2017).
- [24] Spahr, H. *et al.* Imaging pulse wave propagation in human retinal vessels using full-field swept-source optical coherence tomography. *Optics Letters* **40**, 4771 – 4774 (2015).
- [25] Drasdo, N., Millican, C. L., Katholi, C. R. & Curcio, C. A. The length of Henle fibers in the human retina and a model of ganglion receptive field density in the visual field. *Vision Research* **47**, 2901 – 2911 (2007).
- [26] Yau, K. W. Phototransduction mechanism in retinal rods and cones. The Friedenwald Lecture. *Investigative Ophthalmology & Visual Science* **35**, 9 (1994).
- [27] Korenbrot, J. I. & Cone, R. A. Dark ionic flux and the effects of light in isolated rod outer segments. *The Journal of General Physiology* **60**, 20 – 45 (1972).
- [28] Sackmann, E. *Handbook of Biological Physics* (Elsevier, Amsterdam, 1995).
- [29] Cohen, A. I. Electron microscope observations on form changes in photoreceptor outer segments and their saccules in response to osmotic stress. *The Journal of Cell Biology* **48**, 547 – 565 (1971).
- [30] Döbereiner, H.-G., Evans, E., Kraus, M., Seifert, U. & Wortis, M. Mapping vesicle shapes into the phase diagram: A comparison of experiment and theory. *Physics Review E* **55**, 4458 – 4474 (1997).
- [31] Kraft, T. W., Schneeweis, D. M. & Schnapf, J. L. Visual transduction in human rod photoreceptors. *The Journal of Physiology* **464**, 747 – 765 (1993?).
- [32] Sidman, R. L. The structure and concentration of solids in photoreceptor cells studied by refractometry and interference microscopy. *The Journal of Cell Biology* **3**, 15 – 30 (1957).
- [33] Hecht, S., Schlaer, S., Pirenne & Henri, M. Energy, quanta and vision. *Journal of General Physiology* **25**, 819 – 840 (1942).
- [34] Bardy, C. *et al.* Neuronal medium that supports basic synaptic functions and activity of human neurons in vitro. *Proceedings of the National Academy of Sciences* **112**, E2725 – E2734 (2015).
- [35] Liu, Z., Kurokawa, K., Zhang, F., Lee, J. J. & Miller, D. T. Imaging and quantifying ganglion cells and other transparent neurons in the living human retina. *Proceedings of the National Academy of Sciences* **114**, 12803 – 12808 (2017).
- [36] Hillmann, D. *et al.* Aberration-free volumetric high-speed imaging of in vivo retina. *Scientific Reports* **6**, 1–11 (2016).

- [37] Fast Fourier transforms for nonequispaced data: A tutorial. In Benedetto, J. & Ferreira, P. (eds.) *Modern Sampling Theory: Mathematics and Applications*, chap. 12, 249–274 (2001).
- [38] Coifman, R. R. & Lafon, S. Diffusion maps. *Applied and Computational Harmonic Analysis* **21**, 5 – 30 (2006).
- [39] Kafieh, R., Rabbani, H., Abramoff, M. D. & Sonka, M. Intra-retinal layer segmentation of 3D optical coherence tomography using coarse grained diffusion map. *Medical Image Analysis* **17**, 907 – 928 (2013).